

Article

Application of the Single Source—Detector Separation Algorithm in Wearable Neuroimaging Devices: A Step toward Miniaturized Biosensor for Hypoxia Detection

Thien Nguyen, Soongho Park, Jinho Park, Asma Sodager , Tony George  and Amir Gandjbakhche * 

Eunice Kennedy Shriver National Institute of Child Health and Human Development, National Institutes of Health, 49 Convent Drive, Bethesda, MD 20892-4480, USA; thien.nguyen4@nih.gov (T.N.); soongho.park@nih.gov (S.P.); jinho.park@nih.gov (J.P.); asma.sodager@nih.gov (A.S.); tony.george2@nih.gov (T.G.)
* Correspondence: gandjbaa@mail.nih.gov

Abstract: Most currently available wearable devices to noninvasively detect hypoxia use the spatially resolved spectroscopy (SRS) method to calculate cerebral tissue oxygen saturation (StO₂). This study applies the single source—detector separation (SSDS) algorithm to calculate StO₂. Near-infrared spectroscopy (NIRS) data were collected from 26 healthy adult volunteers during a breath-holding task using a wearable NIRS device, which included two source—detector separations (SDSs). These data were used to derive oxyhemoglobin (HbO) change and StO₂. In the group analysis, both HbO change and StO₂ exhibited significant change during a breath-holding task. Specifically, they initially decreased to minimums at around 10 s and then steadily increased to maximums, which were significantly greater than baseline levels, at 25–30 s (p -HbO < 0.001 and p -StO₂ < 0.05). However, at an individual level, the SRS method failed to detect changes in cerebral StO₂ in response to a short breath-holding task. Furthermore, the SSDS algorithm is more robust than the SRS method in quantifying change in cerebral StO₂ in response to a breath-holding task. In conclusion, these findings have demonstrated the potential use of the SSDS algorithm in developing a miniaturized wearable biosensor to monitor cerebral StO₂ and detect cerebral hypoxia.

Keywords: near-infrared spectroscopy; breath holding; cerebral tissue oxygen saturation; cerebral tissue oxygenation; spatially resolved spectroscopy



Citation: Nguyen, T.; Park, S.; Park, J.; Sodager, A.; George, T.; Gandjbakhche, A. Application of the Single Source—Detector Separation Algorithm in Wearable Neuroimaging Devices: A Step toward Miniaturized Biosensor for Hypoxia Detection. *Bioengineering* **2024**, *11*, 385. <https://doi.org/10.3390/bioengineering11040385>

Academic Editors: Dorota Kamińska and Luis Coelho

Received: 1 April 2024
Revised: 12 April 2024
Accepted: 14 April 2024
Published: 16 April 2024



Copyright: © 2024 by the authors. Licensee MDPI, Basel, Switzerland. This article is an open access article distributed under the terms and conditions of the Creative Commons Attribution (CC BY) license (<https://creativecommons.org/licenses/by/4.0/>).

1. Introduction

Hypoxia is characterized by decreased oxygen availability in tissue due to low blood supply or low blood oxygen saturation. Hypoxia includes (1) hypoxemic hypoxia, which is caused by hypoventilation originating from factors such as low oxygen tension at high altitudes, foreign body inhalation, impaired respiratory drive, neuromuscular diseases and an increase in partial pressure of gases other than oxygen; (2) circulatory hypoxia from abnormal cardiac blood flow as seen in left—right shunt; (3) anemic hypoxia due to low hemoglobin concentration; and (4) histotoxic hypoxia, which can be due to causes like cyanide poisoning [1]. Hypoxic brain injury can result from interrupted cerebral blood flow, due to cardiac arrest, strangulation, severe anemia, systemic hypotension, systemic hypoxia [2], or traumatic brain injury [3]. Cerebral hypoxia occurs when cerebral oxygen consumption is larger than oxygen supply due to metabolic needs [4]. Furthermore, this imbalance results from the impaired autoregulation of cerebral blood flow [5,6], which is influenced by mean arterial pressure [7] and intracranial pressure [3]. Hypoxic conditions result in a multitude of involuntary systemic responses to ensure vital organ functioning [8]. Increases in ventilation rate, tidal volume, heart rate, blood pressure, and cerebral blood flow all function in attempting to counteract permanent damage due to hypoxia [8].

The current standard method to monitor patients in an intensive care unit for hypoxia is arterial blood gas analysis (ABG), which requires blood samples to be drawn from a

radial artery [9]. However, the accuracy of an ABG test is affected by barometric pressures and temperatures [10]. Furthermore, blood exposure to air [11] can occur during pneumatic tube transport [12], resulting in an increase in the arterial partial pressure of oxygen [11]. Hemoglobin count is another method to determine hypoxia. A high hemoglobin value can indicate secondary erythrocytosis [13,14], which has been associated with hypoxic lung disease [15,16]. Another measure is jugular vein oxygen saturation (SjvO₂), which increases when the brain oxygen supply exceeds consumption and decreases when consumption exceeds supply. However, this method only provides regional cerebral blood oxygenation [4,17]. Brain Tissue Partial Pressure of Oxygen (PbtO₂) involves the insertion of a microcatheter on the cortex to measure oxygenation as a widely used complement to standard intracranial pressure monitoring [4]. However, it possesses disadvantages such as only providing information about regional ischemia and hypoxia, instead of the entire cortex, posing the risk of injury or infection and requiring significant time to obtain temperature balance after placement prior to data collection [4].

A V/Q scan, also known as a ventilation (V) and perfusion (Q) scan, is an invasive, two-part test involving radiolabeled markers used to indicate the presence of hypoxia [18]. A hypoxia determination is made when there is a V/Q mismatch (low V/Q ratio) as the alveolar oxygen level, also represented as PAO₂, is decreased, which also decreases the arterial oxygen level [1,19]. A single-photon emission computer tomography (SPECT) V/Q scan is particularly useful if patients cannot tolerate a CT scan; however, the Planar Imaging V/Q scan can result in a less accurate determination of pulmonary perfusion [18]. Another method is CT pulmonary angiography, which is used for the diagnosis of pulmonary embolism by identifying structures such as the lung parenchyma and pleural spaces [20]. Many disadvantages of this technique exist, including the degree of patients' ability to hold their breath, which can affect the signal-to-noise ratio, as well as IV access and image timing, which can affect the opaqueness of pulmonary arteries and their quality.

Pulse oximetry is the most common noninvasive method to diagnose patients with hypoxia. However, various factors that cause pulse oximetry readings to become inaccurate include the presence of carboxyhemoglobin and methemoglobin, dark skin pigmentation [21–24], nail polish, dyes, noise from bright lights, electromagnetic interference, motion, low perfusion, sensor location [25], oximeter brand [21,22,26,27] and less sensitivity to non-pulsatile flow [28], and disease [29,30]. Multiple studies have shown greater discrepancies between blood oxygen saturation measured with a pulse oximeter and ABG, particularly for lower oxygenation levels [21–24,29,31–33]. Furthermore, tissue thickness variation can cause different pathlength ratios, which lead to inaccurate readings [34]. Near-infrared spectroscopy (NIRS) is another technique which may be used to evaluate the risk of cerebral ischemia and hypoxia [35]. There are different types of NIRS techniques including continuous-wave (CW) NIRS, time domain (TD) NIRS, and frequency domain (FD) NIRS (fNIRS), with CW NIRS being the most widely available and affordable [4]. The advantage of NIRS over the other techniques of cerebral monitoring include its noninvasiveness, ability for continuous monitoring, and high temporal resolution. So far, five CW NIRS devices have been approved for patient use by the US Food and Drug Administration (FDA), including CerOx (Ornim, Inc., Dedham, MA, USA), EQUANOX 7600 and 8004CA (Nonin Medical, Inc., Plymouth, MN, USA), FORE-SIGHT (CAS Medical Systems, Branford, CT, USA), and INVOS (Somanetics Corporation, Troy, MI, USA) [36]. These devices use the SRS method, which requires at least two source—detector pairs to calculate StO₂.

In our previous study, we derived the single source—detector separation (SSDS) algorithm to calculate StO₂ using information from one source—detector pair [37]. In addition, we have proved its accuracy in StO₂ measurement using both simulation and in vivo data. Simulation data were generated using the Monte Carlo simulation and SSDS-based calculated StO₂ was compared to the actual StO₂. In vivo data were measured from the prefrontal cortex during a hypercapnia task and SSDS-based calculated StO₂ was compared to StO₂ calculated using the SRS method. This study investigates cerebral StO₂ change in response to cerebral hypoxia and compares the sensitivity of the SSDS-based

calculated StO_2 with the SRS-based calculated StO_2 in detecting cerebral hemodynamic change induced by hypoxia. We hypothesize that the SSDS algorithm does not only require less resources than the SRS method to calculate StO_2 but it is also more robust than the SRS method in detecting changes in StO_2 in response to cerebral hypoxia. In this study, a breath-holding task was used to simulate cerebral hypoxia. The aim of the study was to use the SSDS to develop a miniaturized wearable biosensor to monitor cerebral StO_2 , as well as to detect cerebral hypoxia.

2. Materials and Methods

2.1. Participants

The study protocol was approved by the Institutional Review Board of the *Eunice Kennedy Shriver* National Institute of Child Health and Human Development on 31 August 2021 (NICHD protocol #21CH0028), which can be found at clinicaltrials.gov (NCT05035420) (accessed on 1 April 2024). Participant recruitment and experiments were performed from 26 May 2022 to 28 September 2023. This study recruited healthy adult volunteers through the Office of Patient Recruitment at the National Institutes of Health (NIH). The inclusion criteria included (1) participant signature and date on the informed consent form; (2) participant willingness for study procedure compliance and availability for study duration; (3) male or female ≥ 18 years old; (4) good general health confirmed by medical history; (5) no sign of upper respiratory symptoms; and (6) normal range of body temperature on the day of experiment (afebrile, temperature < 100.4 °F). The exclusion criteria for participants included (1) history of skin disease; (2) fever (temperature ≥ 100.4 °F); (3) history of cardiovascular or pulmonary diseases; (4) adverse reactions to latex; (5) any known medical conditions that the principal investigator would not deem safe for participant; (6) inability or unwillingness to provide informed consent; (7) history of respiratory conditions; (8) medication usage that may cause methemoglobinemia; (9) history of smoking or narcotics usage; and (10) ongoing pregnancy. A total of 36 participants (mean age = 38.5 ± 16.5 years old, 23 females) signed written consent forms. After a participant signed the consent form, a physical screening, including a general health and medical history evaluation, an electrocardiogram, and pregnancy test for females of child-bearing age, was performed by a nurse practitioner. Out of 36 participants, 26 (mean age = 34.7 ± 15.7 years old, 18 females) passed the physical screening and were enrolled in the study.

2.2. Experimental Procedures

Because the study was conducted during the COVID-19 pandemic, participants were required to wear a surgical mask throughout the measurement. All experimental procedures were performed in an outpatient clinic at the Clinical Center at the NIH. Before the experiment, measurement devices, including NIRS devices and other equipment, were shown and the experimental procedures were re-explained to participants. Participants were then asked if they wanted to continue participating. After a participant verbally confirmed their willingness to continue, an NIRS device was attached on participants' forehead centered at Fpz location of the 10–20 international system using medical-grade, double-layer tape. During the experiment, participants sat comfortably on a hospital bed and were guided to follow instructions on a screen, which was approximately one meter away. The experiment began with a 5 min rest period, during which participants were asked to relax and breathe normally. A cross sign was displayed at the center of the screen during the first four minutes and a countdown timer was presented during the last minute. The rest period was followed by a breath-holding task. During the task, participants first exhaled and then held their breath for as long as they could within a maximum window of 2 min. The breath-holding task was repeated 3 times interspersed with 2 min rests. Once the breath-holding task was completed, the participants had a 5 min rest period.

2.3. Measurement Device

The hemodynamic responses were measured on participants' forehead using a CW-NIRS device (prototype provided by Hamamatsu photonics K.K., Shizuoka, Japan). The NIRS device consists of a wearable, flexible probe and a portable controller. The probe has a multiwavelength Light-Emitting Diode (LED) operating at 730 nm, 800 nm, and 850 nm and two photodiode detectors that are placed 3 and 4 cm away from the LED. This arrangement forms two different source—detector separations (SDSs) (3 and 4 cm). The overall footprint of the probe is less than 40 cm². The controller is connected to a cell phone for power supply and data recording. The cell phone is integrated with a mobile application to record and process data. Data were recorded at a sampling rate of 120 Hz. The mobile application outputs two worksheets, one for raw data and another for processed data. The processed data include change in oxyhemoglobin (HbO), deoxyhemoglobin (Hb), and total hemoglobin (THb) at each SDS (3 and 4 cm) and tissue oxygen saturation (StO₂), which is calculated using raw data at both separations with the SRS method.

2.4. Data Analysis

Out of 26 recorded data sets, 7 data sets were discarded due to low signal to noise ratios. Among 19 participants with good data, 18 participants performed 3 breath-holding tasks and 1 participant performed 2 breath-holding tasks. Hence, there were total of 56 breath-holding tasks performed. The breath-holding time varied among participants (average time = 41.4 ± 22.4 s; range: 17.5–120 s).

In addition to StO₂ obtained from the mobile application (StO₂-SRS), separate StO₂ values were calculated using the SSDS algorithm (StO₂-SSDS) [37] (Equation (1)). Figure 1 illustrates the SRS method and SSDS algorithm. Backscattered light intensities and initial intensity ratios between wavelengths were extracted from the raw data worksheet. In this study, we used extinction coefficients of HbO and Hb at the three wavelengths reported in [38]. In addition, we assumed that the differential pathlength factor was the same for the three wavelengths (730 nm, 800 nm, and 850 nm).

$$StO_2 = \frac{\langle DPF \rangle_3 \cdot \log(k_1 \cdot I_{\lambda_2} / I_{\lambda_1}) \cdot \epsilon_{\lambda_3}^{Hb} - \langle DPF \rangle_1 \cdot \log(k_2 \cdot I_{\lambda_2} / I_{\lambda_3}) \cdot \epsilon_{\lambda_1}^{Hb} + \langle DPF \rangle_2 \cdot \log(k_2 \cdot I_{\lambda_1} / k_1 \cdot I_{\lambda_3}) \cdot \epsilon_{\lambda_2}^{Hb}}{\langle DPF \rangle_1 \cdot \log(k_2 \cdot I_{\lambda_2} / I_{\lambda_3}) (\epsilon_{\lambda_1}^{HbO} - \epsilon_{\lambda_1}^{Hb}) - \langle DPF \rangle_3 \cdot \log(k_1 \cdot I_{\lambda_2} / I_{\lambda_1}) (\epsilon_{\lambda_3}^{HbO} - \epsilon_{\lambda_3}^{Hb}) + \langle DPF \rangle_2 \cdot \log(k_1 \cdot I_{\lambda_3} / k_2 \cdot I_{\lambda_1}) (\epsilon_{\lambda_2}^{HbO} - \epsilon_{\lambda_2}^{Hb})} \quad (1)$$

where $\langle DPF \rangle_1$ is the differential pathlength factor at wavelength λ_1 , k_1 is the initial intensity ratio between wavelength λ_1 and λ_2 , I_{λ_1} is the backscattered light intensity at wavelength λ_1 , and $\epsilon_{\lambda_1}^{HbO}$ is the extinction coefficient of HbO at wavelength λ_1 .

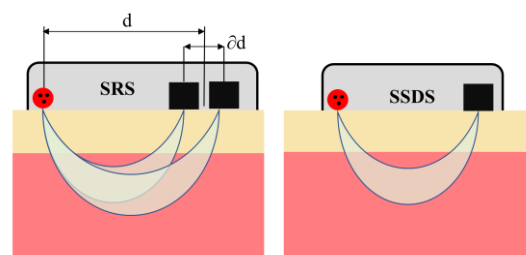


Figure 1. Illustration of devices that use the SRS method and SSDS algorithm. SRS-based devices need to have at least 2 source—detector pairs, while SSDS-based devices need only one source—detector pair; hence, they can be made smaller and simpler. In addition, there is an assumption that d has to be significantly larger than δd in the SRS method. As a result, SRS-based devices need to have detectors far away from the light source, which reduces the signal to noise ratio and increases the device size.

2.5. Statistical Analysis

Hemodynamic responses including HbO change, StO₂-SRS, and StO₂-SSDS were averaged for 5 s for statistical analysis. To eliminate baseline individual variation in

hemodynamic responses, HbO change, StO₂-SRS, and StO₂-SSDS during and after the breath-holding task were subtracted from the baseline data (5 s before the task).

A single-factor one-way analysis of variance (ANOVA) test was performed on the baseline-subtracted, 5 s averaged hemodynamics responses before, during, and after the breath-holding task at different time points. By considering an averaged breath-holding time of 41.4 s, a time range from −5 s (5 s before the task) to 45 s was used. An ANOVA task yielding a *p* value equal to or less than 0.05 was considered statistically significant. Multiple one-sample, two-tailed post hoc *t*-tests (compared to zero) were performed on the baseline-subtracted, 5 s averaged hemodynamics responses during and after the breath-holding task following a significant ANOVA test result. In addition, Pearson correlation coefficients (ρ) among different hemodynamic responses and between the same hemodynamic response at different SDSs were calculated.

3. Results

3.1. HbO Change Due to the Breath-Holding Task

The averaged cerebral HbO changes at the forehead across all participants during and after the breath-holding task are presented in Figure 2. As previously described, the HbO change before, during, and after the task was subtracted from the baseline; hence, the mean and standard errors of HbO change at the baseline (from −5 to 0 s) are zero. During the first 10 s of the breath-holding task, the HbO change from both SDSs gradually decreases to $-0.002 \pm 0.004 \mu\text{M}$ (3 cm SDS) and $-0.003 \pm 0.005 \mu\text{M}$ (4 cm SDS). Between 10–15 s of the task, the HbO change starts increasing and reaches a value greater than the baseline HbO (mean HbO change = $0.005 \pm 0.005 \mu\text{M}$ (3 cm SDS) and $0.007 \pm 0.005 \mu\text{M}$ (4 cm SDS)) at 15–20 s. After that, the HbO change continues to increase until it reaches the maximal peak (mean HbO change = $0.021 \pm 0.005 \mu\text{M}$ (3 cm SDS) and $0.023 \pm 0.005 \mu\text{M}$ (4 cm SDS)) at 25–30 s and then eventually decreases toward the baseline HbO. At 40–45 s, the HbO change is $0.010 \pm 0.005 \mu\text{M}$ (3 cm SDS) and $0.008 \pm 0.005 \mu\text{M}$ (4 cm SDS) above the baseline HbO. A correlation analysis demonstrates that HbO changes from the two SDSs are highly correlated ($\rho = 0.99$). Single-factor one-way ANOVA tests on the baseline-subtracted, 5 s averaged HbO change across 56 breath-holding tasks indicate a significant difference among different times for both 3 cm ($F(9) = 3.7, p < 0.001$) and 4 cm ($F(9) = 4.8, p < 0.001$) SDSs. Post hoc one-sample *t*-tests (compared to zero) show that the HbO change is significantly greater than zero at 20–25 s ($p = 0.02$ (3 cm SDS) and $p = 0.005$ (4 cm SDS)), 25–30 s ($p < 0.001$ (3 and 4 cm SDSs)), 30–35 s ($p = 0.002$ (3 cm SDS) and $p < 0.001$ (4 cm SDS)), and 35–40 s ($p = 0.007$ (3 cm SDS) and $p = 0.005$ (4 cm SDS)).

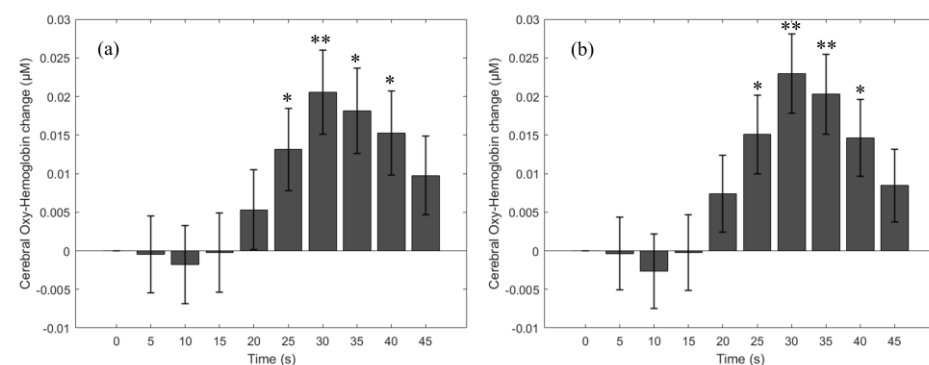


Figure 2. Cerebral HbO changes due to the breath-holding task; (a) HbO change from 3 cm SDS; (b) HbO change from 4 cm SDS. Error bars represent standard error. * indicates a *p* value < 0.05 and ** indicates a *p* value < 0.001.

3.2. Cerebral StO₂-SRS Change Due to the Breath-Holding Task

Similar to HbO, the cerebral StO₂-SRS initially decreases during the first 10 s (mean StO₂-SRS change = $-0.10 \pm 0.17\%$) and gradually increases after that (Figure 3). Between

15–20 s of the task, the cerebral $\text{StO}_2\text{-SRS}$ is greater than the baseline StO_2 (mean $\text{StO}_2\text{-SRS}$ change = $0.24 \pm 0.19\%$). The maximum $\text{StO}_2\text{-SRS}$ change is $0.48 \pm 0.21\%$ at 25–30 s. Eventually, the $\text{StO}_2\text{-SRS}$ decreases toward the baseline $\text{StO}_2\text{-SRS}$. At 40–45 s, the $\text{StO}_2\text{-SRS}$ is $0.24 \pm 0.23\%$ below the baseline $\text{StO}_2\text{-SRS}$. A single factor one-way ANOVA test on the baseline-subtracted, 5 s averaged $\text{StO}_2\text{-SRS}$ across 56 breath-holding tasks indicates a significant difference among different times ($F(9) = 3.3$, $p < 0.001$). Post hoc one-sample t -tests (compared to zero) show that $\text{StO}_2\text{-SRS}$ is significantly greater than zero at 25–30 s ($p = 0.03$). A correlation analysis between the HbO change and $\text{StO}_2\text{-SRS}$ change shows that the $\text{StO}_2\text{-SRS}$ change is greater correlated to the HbO change from 4 cm SDS ($\rho = 0.81$) than the HbO change from 3 cm SDS ($\rho = 0.73$).

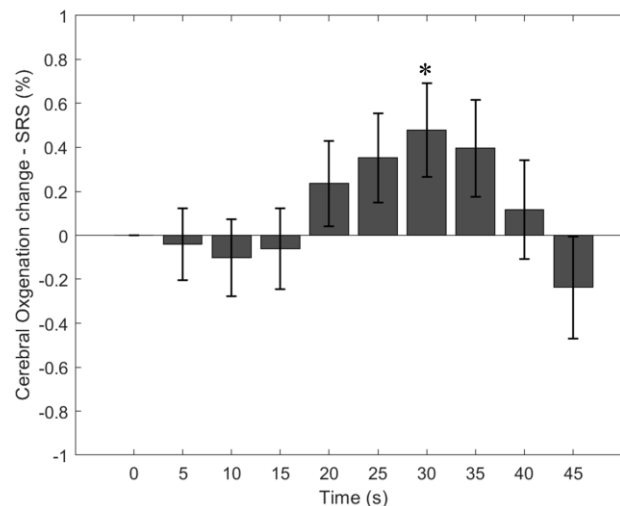


Figure 3. Change in $\text{StO}_2\text{-SRS}$ due to the breath-holding task. Error bars represent standard error. * indicates a p value < 0.05 . $\text{StO}_2\text{-SRS}$ change was obtained from the processed data worksheet.

3.3. Cerebral $\text{StO}_2\text{-SSDS}$ Change Due to the Breath-Holding Task

Due to a low signal to noise ratio, data at 4 cm SDS from one participant were excluded. As a result, $\text{StO}_2\text{-SSDS}$ at 3 cm SDS consists of data from 56 breath-holding tasks, but $\text{StO}_2\text{-SSDS}$ at 4 cm SDS consists of data from 53 breath-holding tasks. Figure 4 represents cerebral $\text{StO}_2\text{-SSDS}$ change in response to the breath-holding task, which has a similar trend to HbO and $\text{StO}_2\text{-SRS}$. Cerebral $\text{StO}_2\text{-SSDS}$ from both SDSs gradually decreases during the first 10 s to $-0.04 \pm 0.4\%$ (3 cm SDS) and $-0.06 \pm 0.3\%$ (4 cm SDS). It then steadily increases to the maximal peak at 25–30 s (mean $\text{StO}_2\text{-SSDS}$ change = $1.22 \pm 0.56\%$ (3 cm SDS) and $0.82 \pm 0.33\%$ (4 cm SDS)). After that, it eventually decreases toward the baseline $\text{StO}_2\text{-SSDS}$. At 40–45 s, $\text{StO}_2\text{-SSDS}$ is $0.54 \pm 0.58\%$ above the baseline $\text{StO}_2\text{-SSDS}$ (3 cm SDS) and $0.17 \pm 0.39\%$ below the baseline $\text{StO}_2\text{-SSDS}$ (4 cm SDS). An analysis between HbO and $\text{StO}_2\text{-SSDS}$ indicates a higher correlation between the two parameters at 3 cm SDS ($\rho = 0.99$) than at 4 cm SDS ($\rho = 0.87$). The correlation coefficients between HbO and $\text{StO}_2\text{-SSDS}$ are higher than the ones between HbO and $\text{StO}_2\text{-SRS}$. An analysis between $\text{StO}_2\text{-SRS}$ and $\text{StO}_2\text{-SSDS}$ shows that $\text{StO}_2\text{-SRS}$ is more correlated with $\text{StO}_2\text{-SSDS}$ at 4 cm SDS ($\rho = 0.98$) than with $\text{StO}_2\text{-SSDS}$ at 3 cm SDS ($\rho = 0.78$).

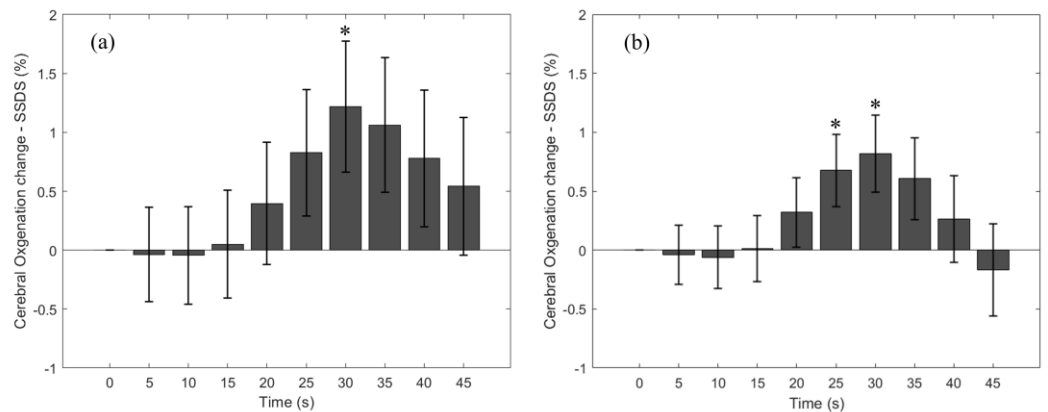


Figure 4. Change in StO₂-SSDS due to the breath-holding task. (a) StO₂-SSDS calculated from 3 cm SDS; (b) StO₂-SSDS calculated from 4 cm SDS. Error bars represent standard error. * indicates a *p* value < 0.05.

3.4. Cerebral StO₂ during a Long versus Short Breath-Holding Task

Figure 5 shows cerebral StO₂ at the forehead during a breath-holding task in two representative participants, who were able to hold their breath for 25 s (duration indicated by vertical lines, Figure 5a) and 120 s (duration indicated by vertical lines, Figure 5b). In both participants, cerebral StO₂ initially decreased to a minimal level and then gradually increased to an StO₂ level greater than the resting StO₂ at the end of the task. However, in the participant with a short hold (25 s), StO₂ was decreasing continuously for approximately 5 s, but in the participant with a long hold (120 s), StO₂ was decreasing continuously for approximately 15 s. In addition, after reaching its minimal peak, StO₂ steadily increased until the end of the task in a short hold, but in a long hold, StO₂ fluctuated greatly. Comparing between StO₂-SRS (yellow trace) and StO₂-SSDS (blue and red traces), StO₂ alteration in response to a long hold is similar between SRS and SSDS (Figure 5). However, StO₂ alteration in response to a short hold is more observable in StO₂-SSDS than in StO₂-SRS. Specifically, at 5 s, StO₂-SSDS decreases by 0.84% (3 cm SDS) and 0.94% (4 cm SDS), while StO₂-SRS decreases only 0.51% from the resting StO₂. Moreover, at the end of the task, StO₂-SSDS increases 2.71% (3 cm SDS) and 1.65% (4 cm SDS), while StO₂-SRS increases only 0.03% from the resting StO₂. The small change in StO₂-SRS in response to a short breath-holding task makes it indistinguishable from background variation during rest. Furthermore, StO₂-SRS has lower signal to noise ratio compared to StO₂-SSDS at both SDSs and StO₂-SRS shares the same artifacts (spikes) with StO₂-SSDS at 4 cm SDS, in both the short and long breath-holding tasks (Figure 5).

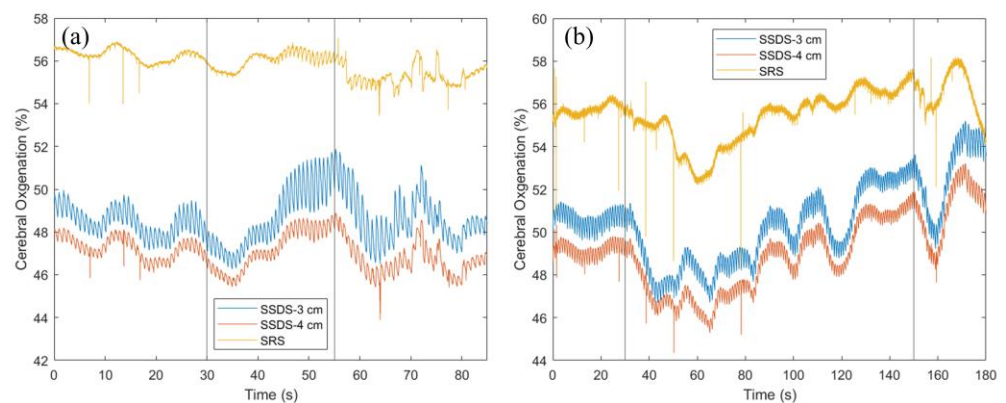


Figure 5. StO₂-SRS and StO₂-SSDS before, during, and after a breath-holding task; (a) short task and (b) long task. Vertical lines mark the start and end of the breath-holding task.

4. Discussion

In this study, we measured cerebral hemodynamic responses, including HbO change and StO₂, during a breath-holding task. Cerebral StO₂ was derived from two different methods, namely SRS and SSDS. We have shown that both HbO change and StO₂ initially decrease to a minimal peak at around 10 s of the breath-holding task and then steadily increase to a maximum peak, which is significantly greater than the baseline level, at 25–30 s. Comparing between SRS and SSDS, we have demonstrated that SSDS is more robust than SRS in quantifying changes in cerebral StO₂ in response to a breath-holding task. In addition, we found that StO₂-SSDS has a higher correlation with HbO change than StO₂-SRS.

Our result of hemodynamic responses to a breath-holding task is consistent with previous studies, in which controlled breath holding was used to model the systemic physiological effects of hypoxia in patients [39,40]. The act of breath holding leads to a decrease in the partial pressure of oxygen and a rise in carbon dioxide (CO₂) above the normative value of around 40 mmHg [40]. This change can damage vital organs such as the brain. As a result, to protect the brain, a compensatory neurovascular response occurs to provide a constant supply of oxygen to the brain through increased cerebral blood flow [1]. This increased neurovascular blood flow is achieved through dilation of intracranial and extracranial blood vessels [1–3], particularly in the middle cerebral artery which supports this compensatory response [21]. However, the response can only be maintained for a limited time as neural tissue death can occur in under 3 min when the supply of oxygen is interrupted [4]. The hypoxic responses to breath holding can happen in as little as 5 s where peripheral oxygen saturation drops continuously. In contrast, the cerebral tissue oxygen saturation will immediately drop at the start of the event but subsequently recovers to a level slightly above the baseline [39].

Even though there is an observable trend in hemodynamic responses to the breath-holding task and the trend is similar to previous studies, there is a large standard error throughout the task. In particular, the standard error tends to increase toward the end of the task. The large standard error could be because of the difference in individual hemodynamic responses to the task and breath-holding duration between participants. For example, the cerebral StO₂ reaches its minimal peak at an earlier time and with a smaller amplitude in a short hold compared to a long hold. In addition, from 5 s to 15 s, StO₂ is continuously decreasing during a long hold, but it is steadily increasing in a short hold. In contrast to the change at the beginning of the breath-holding task, the cerebral StO₂ increases and reaches its maximal peak at the end of the task. Thus, after 25 s, cerebral StO₂ starts decreasing towards the baseline in a short hold, but it continues to increase in a long hold.

The results of this study indicate that SSDS is better than SRS in monitoring changes in cerebral StO₂ in response to a breath-holding task. Firstly, SSDS is able to more accurately detect change in cerebral StO₂ in response to a short breath-holding task, while SRS fails to do so. Secondly, StO₂-SSDS at 4 cm SDS is highly correlated with StO₂-SRS and StO₂-SRS shares the same artifacts with StO₂-SSDS at 4 cm SDS. Due to the far distance between a light source and a photodetector at 4 cm SDS, both SRS and SSDS at 4 cm SDS suffers from a low signal to noise ratio, especially in a tissue with high absorption. Thirdly, due to an assumption that the distance between photodetectors is substantially smaller than the distance between the light source and photodetectors in SRS, photodetectors often should be placed far away from the light source. As a result, SRS cannot be used to quantify oxygen saturation at superficial tissues, making contamination from the scalp and skull unavoidable. On the other hand, SSDS can be applied on a close SDS (for example SDS < 1 cm) to calculate the StO₂ of superficial tissues, which can be used to eliminate the effect of scalp and skull StO₂ on measured cerebral StO₂. Finally, since SSDS requires information from only one source—detector pair, devices using SSDS can be made smaller and more cost-effective.

Tissue oxygen saturation is a mixture of blood oxygen saturation in arteries, veins, and capillaries. Therefore, depending on the distribution of blood vessels, StO₂ can vary greatly between people. As a result, StO₂ cannot be used to diagnose hypoxia. However, it can be used in a monitoring manner for daily use or neurosurgery.

5. Conclusions

This study applies the single source—detector separation algorithm to calculate cerebral tissue oxygen saturation during a breath-holding task. We have proved that this algorithm is better than the conventional spatially resolved spectroscopy method in detecting and quantifying alterations in cerebral tissue oxygen saturation in response to a breath-holding task. In addition, because the single source—detector separation algorithm requires information from only one source—detector pair, it can be a great candidate for a miniaturized biosensor to monitor tissue oxygen saturation as well as to detect hypoxia. The miniaturized biosensor can not only be used as a standalone wearable device for monitoring tissue oxygen saturation noninvasively but it can also be attached on an endoscope for measuring the oxygen saturation of internal organs. The wearable device can be used to detect hypoxia in divers, people living at high altitudes, and patients undergoing neurosurgery. The endoscopic biosensor can be used to study the oxygen saturation of inflamed areas or cancer tissues.

Author Contributions: Conceptualization, T.N. and A.G.; Methodology, T.N., S.P., J.P. and A.G.; Software, T.N., S.P. and J.P.; Validation, T.N., S.P., J.P. and A.G.; Formal Analysis, T.N.; Investigation, T.N. and A.G.; Resources, A.G.; Data Curation, T.N.; Writing—Original Draft Preparation, T.N., A.S. and T.G.; Writing—Review and Editing, T.N., S.P., J.P., A.S., T.G. and A.G.; Visualization, T.N. and S.P.; Supervision, A.G.; Project Administration, T.N. and A.G.; Funding Acquisition, A.G. All authors have read and agreed to the published version of the manuscript.

Funding: This research was funded by the Intramural Research Program at the Eunice Kennedy Shriver National Institute of Child Health and Human Development, National Institutes of Health, grant number [Z01-HD000261].

Institutional Review Board Statement: The study was conducted according to the guidelines of the Declaration of Helsinki and approved by the Institutional Review Board of the *Eunice Kennedy Shriver* National Institute of Child Health and Human Development on 31 August 2021 (NICHD protocol #21CH0028).

Informed Consent Statement: Informed consent was obtained from all subjects involved in the study.

Data Availability Statement: Data supporting the reported results will be uploaded to Github upon publication.

Acknowledgments: We acknowledge Hamamatsu Photonics Company and the Section on Biomedical Optics at NICHD for lending us their CW-NIRS prototype to conduct experiments.

Conflicts of Interest: The authors declare no conflicts of interest.

References

1. Bhutta, B.S.; Alghoula, F.; Berim, I. Hypoxia. In *StatPearls*; StatPearls Publishing LLC.: Treasure Island, FL, USA, 2024.
2. Lacerte, M.; Hays Shapshak, A.; Mesfin, F.B. Hypoxic Brain Injury. In *StatPearls*; StatPearls Publishing LLC.: Treasure Island, FL, USA, 2024.
3. Barud, M.; Dabrowski, W.; Siwicka-Gieroba, D.; Robba, C.; Bielacz, M.; Badenes, R. Usefulness of Cerebral Oximetry in TBI by NIRS. *J. Clin. Med.* **2021**, *10*, 2938. [[CrossRef](#)] [[PubMed](#)]
4. Zhong, W.; Ji, Z.; Sun, C. A Review of Monitoring Methods for Cerebral Blood Oxygen Saturation. *Healthcare* **2021**, *9*, 1104. [[CrossRef](#)] [[PubMed](#)]
5. Lam, J.M.K.; Hsiang, J.N.K.; Poon, W.S. Monitoring of autoregulation using laser Doppler flowmetry in patients with head injury. *J. Neurosurg.* **1997**, *86*, 438–445. [[CrossRef](#)] [[PubMed](#)]
6. Rivera-Lara, L.; Zorrilla-Vaca, A.; Geocadin, R.G.; Healy, R.J.; Ziai, W.; Mirski, M.A. Cerebral Autoregulation-oriented Therapy at the Bedside: A Comprehensive Review. *Anesthesiology* **2017**, *126*, 1187–1199. [[CrossRef](#)] [[PubMed](#)]

7. Brady, K.M.; Lee, J.K.; Kibler, K.K.; Smielewski, P.; Czosnyka, M.; Easley, R.B.; Koehler, R.C.; Shaffner, D.H. Continuous time-domain analysis of cerebrovascular autoregulation using near-infrared spectroscopy. *Stroke* **2007**, *38*, 2818–2825. [[CrossRef](#)] [[PubMed](#)]
8. Kane, A.D.; Kothmann, E.; Giussani, D.A. Detection and response to acute systemic hypoxia. *BJA Educ.* **2020**, *20*, 58–64. [[CrossRef](#)] [[PubMed](#)]
9. Gattinoni, L.; Pesenti, A.; Matthay, M. Understanding blood gas analysis. *Intensive Care Med.* **2018**, *44*, 91–93. [[CrossRef](#)] [[PubMed](#)]
10. Castro, D.; Patil, S.M.; Zubair, M.; Keenaghan, M. Arterial Blood Gas. In *StatPearls*; StatPearls Publishing LLC.: Treasure Island, FL, USA, 2024.
11. Lima-Oliveira, G.; Lippi, G.; Salvagno, G.L.; Montagnana, M.; Picheth, G.; Guidi, G.C. Different manufacturers of syringes: A new source of variability in blood gas, acid-base balance and related laboratory test? *Clin. Biochem.* **2012**, *45*, 683–687. [[CrossRef](#)] [[PubMed](#)]
12. Albert, T.J.; Swenson, E.R. Circumstances When Arterial Blood Gas Analysis Can Lead Us Astray. *Respir Care* **2016**, *61*, 119–121. [[CrossRef](#)]
13. Haider, M.Z.; Anwer, F. Secondary Polycythemia. In *StatPearls*; StatPearls Publishing LLC.: Treasure Island, FL, USA, 2023.
14. Billett, H.H. Hemoglobin and Hematocrit. In *Clinical Methods: The History, Physical, and Laboratory Examinations*; Walker, H.K., Hall, W.D., Hurst, J.W., Eds.; Butterworth Publishers, a division of Reed Publishing: Boston, MA, USA, 1990.
15. Mithoowani, S.; Laureano, M.; Crowther, M.A.; Hillis, C.M. Investigation and management of erythrocytosis. *Cmaj* **2020**, *192*, E913–E918. [[CrossRef](#)]
16. Sakisaka, S.; Watanabe, M.; Tateishi, H.; Harada, M.; Shakado, S.; Mimura, Y.; Gondo, K.; Yoshitake, M.; Noguchi, K.; Hino, T.; et al. Erythropoietin production in hepatocellular carcinoma cells associated with polycythemia: Immunohistochemical evidence. *Hepatology* **1993**, *18*, 1357–1362. [[CrossRef](#)]
17. Bouzat, P.; Sala, N.; Payen, J.F.; Oddo, M. Beyond intracranial pressure: Optimization of cerebral blood flow, oxygen, and substrate delivery after traumatic brain injury. *Ann. Intensive Care* **2013**, *3*, 23. [[CrossRef](#)]
18. Mirza, H.; Hashmi, M.F. Lung Ventilation Perfusion Scan (VQ Scan). In *StatPearls*; StatPearls Publishing LLC.: Treasure Island, FL, USA, 2024.
19. Sarkar, M.; Niranjana, N.; Banyal, P.K. Mechanisms of hypoxemia. *Lung India* **2017**, *34*, 47–60. [[CrossRef](#)]
20. Soye, J.A.; Loughrey, C.B.; Hanley, P.D. Computed tomography pulmonary angiography: A sample of experience at a District General Hospital. *Ulster Med. J.* **2008**, *77*, 175–180.
21. Bickler, P.E.; Feiner, J.R.; Severinghaus, J.W. Effects of skin pigmentation on pulse oximeter accuracy at low saturation. *J. Am. Soc. Anesthesiol.* **2005**, *102*, 715–719. [[CrossRef](#)]
22. Feiner, J.R.; Severinghaus, J.W.; Bickler, P.E. Dark skin decreases the accuracy of pulse oximeters at low oxygen saturation: The effects of oximeter probe type and gender. *Anesth. Analg.* **2007**, *105*, S18–S23. [[CrossRef](#)] [[PubMed](#)]
23. Wong, A.-K.I.; Charpignon, M.; Kim, H.; Josef, C.; De Hond, A.A.; Fojas, J.J.; Tabaie, A.; Liu, X.; Mireles-Cabodevila, E.; Carvalho, L. Analysis of discrepancies between pulse oximetry and arterial oxygen saturation measurements by race and ethnicity and association with organ dysfunction and mortality. *JAMA Netw. Open* **2021**, *4*, e2131674. [[CrossRef](#)] [[PubMed](#)]
24. Crooks, C.J.; West, J.; Morling, J.R.; Simmonds, M.; Juurlink, I.; Briggs, S.; Cruickshank, S.; Hammond-Pears, S.; Shaw, D.; Card, T.R. Pulse oximeter measurement error of oxygen saturation in patients with SARS-CoV-2 infection stratified by smoking status. *Eur. Respir. J.* **2022**, *60*, 2201190. [[CrossRef](#)] [[PubMed](#)]
25. Sedaghat-Yazdi, F.; Torres, A., Jr.; Fortuna, R.; Geiss, D.M. Pulse oximeter accuracy and precision affected by sensor location in cyanotic children. *Pediatr. Crit. Care Med.* **2008**, *9*, 393–397. [[CrossRef](#)]
26. Foglia, E.E.; Whyte, R.K.; Chaudhary, A.; Mott, A.; Chen, J.; Propert, K.J.; Schmidt, B. The effect of skin pigmentation on the accuracy of pulse oximetry in infants with hypoxemia. *J. Pediatr.* **2017**, *182*, 375–377.e372. [[CrossRef](#)]
27. Harris, B.U.; Char, D.S.; Feinstein, J.A.; Verma, A.; Shiboski, S.C.; Ramamoorthy, C. Accuracy of pulse oximeters intended for hypoxemic pediatric patients. *Pediatr. Crit. Care Med.* **2016**, *17*, 315–320. [[CrossRef](#)] [[PubMed](#)]
28. Yuan, H.; Palmer, G.M.; Dewhirst, M.W. Chapter 46—Imaging Hypoxia. In *Molecular Imaging*, 2nd; Ross, B.D., Gambhir, S.S., Eds.; Academic Press: Cambridge, MA, USA, 2021; pp. 869–895. [[CrossRef](#)]
29. Nguyen, L.S.; Helias, M.; Raia, L.; Nicolas, E.; Jaubert, P.; Benghanem, S.; Ait Hamou, Z.; Dupland, P.; Charpentier, J.; Pène, F. Impact of COVID-19 on the association between pulse oximetry and arterial oxygenation in patients with acute respiratory distress syndrome. *Sci. Rep.* **2022**, *12*, 1462. [[CrossRef](#)] [[PubMed](#)]
30. Pu, L.J.; Shen, Y.; Lu, L.; Zhang, R.Y.; Zhang, Q.; Shen, W.F. Increased blood glycohemoglobin A1c levels lead to overestimation of arterial oxygen saturation by pulse oximetry in patients with type 2 diabetes. *Cardiovasc. Diabetol.* **2012**, *11*, 110. [[CrossRef](#)]
31. Wilson, B.J.; Cowan, H.J.; Lord, J.A.; Zuege, D.J.; Zygun, D.A. The accuracy of pulse oximetry in emergency department patients with severe sepsis and septic shock: A retrospective cohort study. *BMC Emerg. Med.* **2010**, *10*, 9. [[CrossRef](#)] [[PubMed](#)]
32. Ross, P.A.; Newth, C.J.; Khemani, R.G. Accuracy of pulse oximetry in children. *Pediatrics* **2014**, *133*, 22–29. [[CrossRef](#)] [[PubMed](#)]
33. Ascha, M.; Bhattacharyya, A.; Ramos, J.A.; Tonelli, A.R. Pulse oximetry and arterial oxygen saturation during cardiopulmonary exercise testing. *Med. Sci. Sports Exerc.* **2018**, *50*, 1992. [[CrossRef](#)] [[PubMed](#)]
34. Petterson, M.T.; Begnoche, V.L.; Graybeal, J.M. The effect of motion on pulse oximetry and its clinical significance. *Anesth. Analg.* **2007**, *105*, S78–S84. [[CrossRef](#)] [[PubMed](#)]

35. Tsai, H.I.; Chung, P.C.; Lee, C.W.; Yu, H.P. Cerebral perfusion monitoring in acute care surgery: Current and perspective use. *Expert. Rev. Med. Devices* **2016**, *13*, 865–875. [[CrossRef](#)] [[PubMed](#)]
36. Yu, Y.; Zhang, K.; Zhang, L.; Zong, H.; Meng, L.; Han, R. Cerebral near-infrared spectroscopy (NIRS) for perioperative monitoring of brain oxygenation in children and adults. *Cochrane Database Syst. Rev.* **2018**, *1*, CD010947. [[CrossRef](#)]
37. Nguyen, T.; Park, S.; Hill, B.; Gandjbakhche, A.H. Single Source-Detector Separation Approach to Calculate Tissue Oxygen Saturation Using Continuous Wave Near-infrared Spectroscopy. *IEEE Open J. Eng. Med. Biol.* **2023**, *4*, 79–84. [[CrossRef](#)]
38. Zijlstra, W.G.; Buursma, A.; der Roest, W.P.M.-V. Absorption spectra of human fetal and adult oxyhemoglobin, de-oxyhemoglobin, carboxyhemoglobin, and methemoglobin. *Clin. Chem.* **1991**, *37*, 1633–1638. [[CrossRef](#)] [[PubMed](#)]
39. Bouten, J.; Bourgois, J.G.; Boone, J. Hold your breath: Peripheral and cerebral oxygenation during dry static apnea. *Eur. J. Appl. Physiol.* **2020**, *120*, 2213–2222. [[CrossRef](#)] [[PubMed](#)]
40. Parkes, M.J. Breath-holding and its breakpoint. *Exp. Physiol.* **2006**, *91*, 1–15. [[CrossRef](#)] [[PubMed](#)]

Disclaimer/Publisher’s Note: The statements, opinions and data contained in all publications are solely those of the individual author(s) and contributor(s) and not of MDPI and/or the editor(s). MDPI and/or the editor(s) disclaim responsibility for any injury to people or property resulting from any ideas, methods, instructions or products referred to in the content.